npj | clean water

Article

Published in partnership with King Fahd University of Petroleum & Minerals

https://doi.org/10.1038/s41545-024-00387-6

Joule and photothermal heating techniques for oil desorption with techno-economic feasibility and environmental impact analysis

Siyoung Byun[1], Muhammad Usman Farid[2,3], Nallapaneni Manoj Kumar[2,4], Shauhrat S. Chopra[2], Sangyong Nam[5], Alicia Kyoungjin An[2,3] ✉ & Sanghyun Jeong[1] ✉

Joule and photothermal heating offer promising avenues for enhancing oil recovery, desorption, and reusability by reducing the viscosity of highly viscous oils, thereby facilitating their mobility on sorbent surface. This study developed a heatable reduced graphene oxide nanoribbon (r-GONR)-coated polyvinylidene fluoride (PVDF) oil sorbent to address these viscosity challenges. The application of heating increased oil desorption by approximately 50%, significantly outperforming the conventional PVDF mat. The r-GONR sorbent, leveraging the photothermal effect, demonstrated exceptional reusability, maintaining 40% oil desorption efficiency up to the 10th cycle. Furthermore, its high oil desorption and reusability translated into considerable economic benefits, with a revenue potential of 6.4–29.0 $/m^2, alongside significant environmental impact reduction. This study introduces a novel, sustainable approach to oil desorption and reuse, underscoring the practical applications of heatable materials in enhancing oil recovery.

According to the Statistical Review of World Energy (2023), global oil consumption has steadily increased over the last three decades, reaching 4.39 billion metric tons. This increase has been attributed to the development of transportation and various other industries, including textiles, petrochemicals, and pharmaceuticals[1–3]. However, the amount of oil leakage and spills has increased owing to increased oil consumption, transportation, processing, and exploration, resulting in water contamination by accidental oil leakage and spills[4,5]. Therefore, prompt and highly efficient oil clean-up is required to minimise the severe damage to the ecosystem and loss to human society caused by water pollution[6].

Polymeric sorbents are highly valued for their oil/water selectivity, removal efficiency, cost-effectiveness in oil spill clean-up, and easy processing[7–11]. However, conventional polypropylene (PP) sorbents face challenges in terms of oil desorption and reusability because of the strong adhesion of highly viscous crude oil[12,13]. The disposal of single-use sorbents by incineration and landfill poses environmental and economic concerns[14,15]. Addressing these issues necessitates the development of sustainable and reusable materials and methodologies for oil cleanup. In addition, the reuse and sustainability of oil sorbents, as well as oil recovery and recycling, are crucial for conserving valuable resources. Oil recovered from sorbents *via* desorption can lead to significant cost savings and generate revenue through recycling. This process not only conserves resources but also mitigates pollution and reduces the costs associated with waste treatment of unrecovered oil[16].

Previous studies have demonstrated that heating can effectively facilitate oil desorption and enhance sorbent reusability and oil recovery by reducing oil viscosity[17]. For instance, the viscosity of crude oil decreases significantly at elevated temperatures, promoting oil fluidity and efficient desorption from sorbent[18,19]. Typically, crude oil, characterised by high viscosity, exhibits a viscosity of approximately 15,000 mPa·s at room temperature, which diminishes to approximately 1300 mPa·s at an oil temperature of 50 °C[20,21]. This reduction in viscosity promoted oil fluidity, facilitating its flow on the surface and efficient desorption from the sorbent[22].

[1]Civil and Environmental Engineering, Pusan National University, Busan, Republic of Korea. [2]School of Energy and Environment, City University of Hong Kong, Kowloon, Hong Kong, China. [3]Department of Chemical and Biological Engineering, The Hong Kong University of Science and Technology, Clear Water Bay, Hong Kong, China. [4]Center for Resource Recovery, HICCER – Hariterde International Council of Circular Economy Research, Palakkad, Kerala, India. [5]Department of Materials Engineering and Convergence Technology, Gyeongsang National University, Jinju, Republic of Korea. ✉e-mail: alicia.kjan@ust.hk; sh.jeong@pusan.ac.kr

In recent years, heatable oil polymeric sorbents have emerged to exploit the heating effects and improve oil mobility *via* Joule-heating, photothermal processes, or magnetocaloric effects induced by external energy sources such as electricity, solar radiation, or magnetic properties, resulting in augmented oil diffusion coefficients[22–26]. While magnetocaloric technology can generate heat within the oil sorbent, thereby decreasing oil viscosity through magnetic heating[27], its practical application is impeded by challenges such as costly materials, magnets, and the instability of magnetocaloric materials[28,29]. Conversely, the Joule-heating effect converts electric energy into thermal energy through intrinsic collisions between phonons and electrons, whereas photothermal technology transforms adsorbed solar radiation into thermal energy[30,31]. Consequently, these technologies reduce oil viscosity and increase the diffusion coefficient, offering operational simplicity and versatility[21,32]. Therefore, this study utilised Joule and photothermal heating technologies for oil desorption and sorbent reuse.

To fabricate materials suitable for Joule-heating or photothermal (or solar-assisted heating) methods, various carbon-based materials, including carbon nanotubes, graphene, MXene, and graphene nanoribbons (GNRs), have been employed[33–37]. An exemplary heatable wood sponge incorporating fluoroalkyl silane-modified reduced graphene oxide (GO) achieved a temperature of 112.8 °C at 20 V[38]. Furthermore, Huang et al.[39] reported a multi-walled carbon nanotube (MWCNT)/polyvinylidene fluoride and polydimethylsiloxane membrane attaining a temperature of 85.1 °C under 1 $kW{\cdot}m^{-1}$. Guo et al.[40] synthesised GO-functionalised polyvinyl alcohol electrospun fibrous membranes exhibiting a high surface temperature of approximately 50 °C under 1 sun. Among the array of carbon-based materials, graphene oxide nanoribbons (GONRs), characterised by elongated strips of graphene, stand out as a promising component for Joule and photothermal heating owing to their high electrical conductivity, thermal resistance, excellent thermal efficiency, and hydrophobicity/oleophilicity[41–44]. They also demonstrated favourable photothermal conversion properties attributed to strong near-infrared (NIR) light adsorption[45]. In addition, the exceptional mechanical and chemical stabilities of reduced-GONR (r-GONR) ensure that they remain effective for sorbing and desorbing oil even under high-temperature conditions (i.e., heating)[46–48].

In this study, a method involving the coating of a heatable r-GONR onto a polyacrylonitrile fluoride (PVDF) oil sorbent was developed to enhance the solar and Joule-heating-assisted desorption and oil recovery of highly viscous oil, to improve the electrical conductivity, thermal resistance, and hydrophobicity/oleophilicity. Initially, a PVDF mat was fabricated *via* electrospinning to achieve high specific surface area and hydrophobic characteristics. Subsequently, r-GONRs were applied to the surface of the PVDF mat to augment the electrical conductivity and thermal resistance. Specifically, we sought to present viable technologies for oil desorption (reusability) by employing Joule-heating and photothermal effects at 25 V and 1 kW/m^2, respectively. The oil desorption capacity, removal efficiency, and reusability were evaluated using highly viscous oils, such as the motor oils 5 W-40 and 10 W-40, and light oils, including diesel oil.

Furthermore, economic and environmental impact assessments were conducted to emphasise the net benefits in terms of both profitability and environmental sustainability. The economic assessment focused on revenue and profitability to validate the viability of oil desorption and reuse methods *via* Joule-heating and photothermal technologies. This was achieved by comparing the performance of the heatable r-GONR oil sorbents with that of non-heatable PVDF mats and commercial PP sorbents. The environmental impact assessment primarily addresses the mitigation of selected environmental impacts specific to oil spill applications. These effects include climate change, fossil fuel depletion, freshwater and marine ecotoxicity, and water depletion.

Results and discussion

Fabrication of heatable oil sorbent

A heatable oil sorbent coated with r-GONRs was fabricated by dip- and spray-coating onto an electrospun PVDF mat. The electrospun PVDF mat showed a nanofibrous structure with an average fibre diameter of 0.56 μm, while the r-GONR oil sorbent exhibited complete surface coverage with r-GONR (Fig. 1a, b). Confirmation of the r-GONR coating was achieved *via* scanning electron microscopy-energy dispersive spectroscopy (SEM-EDS) elemental mapping, where the PVDF mat revealed the presence of F, which is a characteristic of PVDF (Fig. 1c). By contrast, the r-GONR-coated sorbent displayed elements C and O, attributed to the presence of r-GONRs, which were uniformly distributed on the surface (Fig. 1d). Notably, the r-GONR-coated sorbent exhibits lower F levels than the PVDF mat, which is indicative of surface modification. The chemical compositions of the oil sorbents were investigated using X-ray photoelectron spectroscopy. The PVDF mat exhibits distinct C 1 s and F 1 s spectrums [2]. However, after coating the PVDF mat with r-GONRs, the r-GONR oil sorbent exhibited more intense C 1 s and O 1 s peaks. The F 1 s peak disappeared, indicating that the r-GONRs fully coated the PVDF mat (Supplementary Fig. 1). Furthermore,

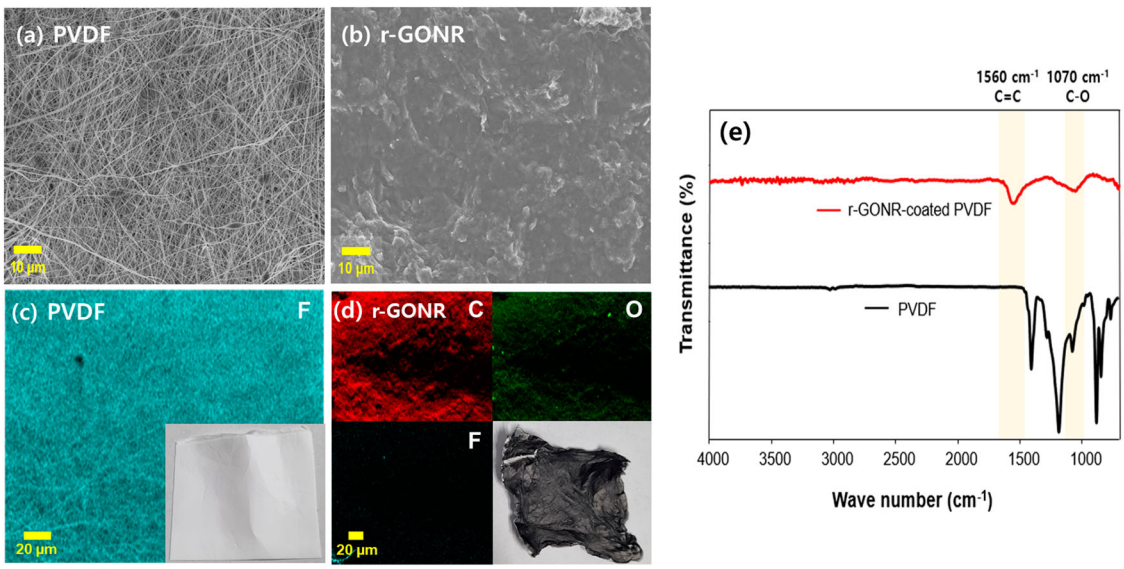

Fig. 1 | Characterization of the PVDF mat and r-GONR oil sorbent. SEM images of (**a**) the PVDF and (**b**) r-GONR oil sorbents, and SEM-EDS elemental mapping images of (**c**) the PVDF and (**d**) r-GONR oil sorbent, and (**e**) FTIR spectra.

Table 1 | Characterisation of the oil sorbents

Oil sorbents	WCA (°)	OCA (°)	Porosity (%)	Tensile strength (MPa)
PVDF	110.55 (±3.34)	0	91.65 (±0.36)	4.69 (±1.18)
r-GONR	100.09 (±8.13)	0	91.10 (±1.21)	6.95(±0.86)

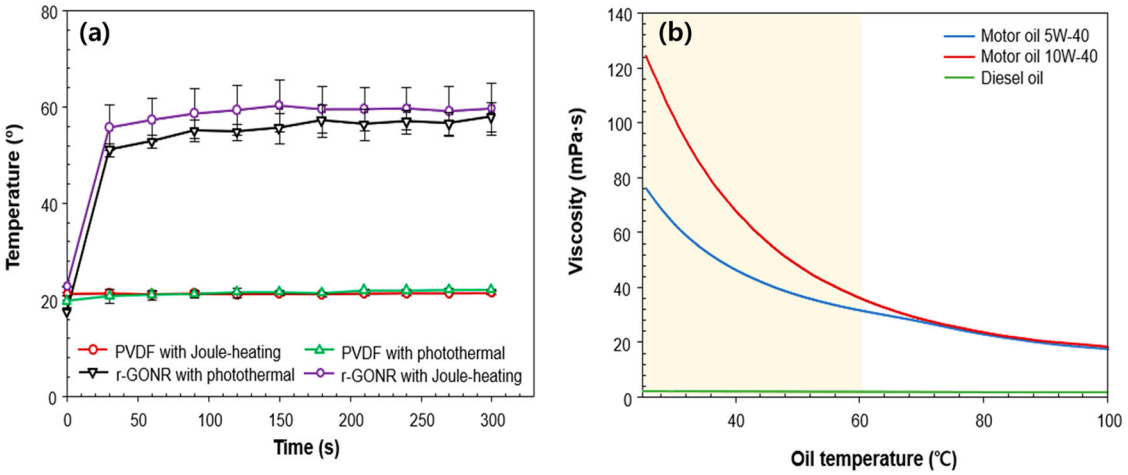

Fig. 2 | For Joule-heating and photothermal effect, thermal performance of the oil sorbent and oil viscosity based on oil temperature. a Thermal performance of the oil sorbents with different heating effects and (**b**) change of oil viscosity with aspect to different oil temperatures with motor oils 5W-40 and 10W-40, and diesel oil (*Each error bar is defined as the standard deviation of the mean.).

distinct chemical compositions, including those of C = C (1560 cm^{-1}) and C–O (1070 cm^{-1}) (Fig. 1e), indicate the presence of a functional group in the r-GONR compared to that in the PVDF mat[17].

Wettability assessment using contact angles with water and oil, denoted as water contact angle (WCA) and oil contact angle (OCA), respectively, revealed that the r-GONR-coated sorbent exhibited slightly lower WCA (110.55 ± 3.34°) compared to the PVDF mat (100.09 ± 8.13°), while maintaining hydrophobicity. Despite the slight decrease in the WCA, the sorbent demonstrated excellent oleophilicity with an OCA of 0°. Additionally, the r-GONR-coated sorbent exhibited comparable porosity (91.10 ± 1.21%) to the PVDF mat (Table 1). To assess the mechanical and chemical stabilities, the tensile strengths of the PVDF mat and r-GONR oil sorbent were evaluated, as shown in Table 1. The r-GONR oil sorbent exhibited a higher tensile strength (6.95 ± 0.86 MPa) compared to the PVDF mat (4.69 ± 1.18 MPa), indicating superior mechanical strength and stability of r-GONR. Chemical stability was tested by exposing the sorbents to solutions with pH values of 2, 4, 6, 9, and 12, as shown in Supplementary Fig. 2. Both sorbents maintained comparable shapes and structures after 1 h, demonstrating their robust chemical stabilities over a range of pH values.

The thermal performance of the sorbents was evaluated using Joule-heating and photothermal effects (Fig. 2a). The surface temperature of the PVDF mat remained unchanged with both Joule-heating and photothermal effects, measuring 21.3 ± 0.3 °C and 22.0 ± 0.1 °C, respectively. This is attributed to its poor electrical conductivity (~10^{-12} S/cm)[49]. Conversely, the r-GONR oil sorbent showed a significant increase in surface temperature under solar-assisted heating, reaching 51.0 ± 1.2 °C within 30 s and gradually rising to 57.8 ± 3.0 °C. Upon applying the Joule-heating effect at different voltages (20 to 30 V), the surface temperature of the r-GONR oil sorbent escalated to 94.6 °C (Supplementary Fig. 3). Remarkably, Joule-heating at 25 V achieved a comparable surface temperature (59.6 ± 5.4 °C) to solar-assisted heating (57.8 ± 3.0 °C). Thus, this condition was selected for a comparative analysis of the oil desorption outcomes between the Joule-heating and photothermal effects.

In Fig. 2b, the oil viscosities are depicted at different oil temperatures. Highly viscous oils such as motor oils 5W-40 and 10W-40 showed decreased viscosity with increasing temperature, particularly experiencing a rapid decrease at nearly 60 °C. Consequently, it is anticipated that both Joule-heating-assisted heat at 25 V and solar-assisted heat at 1 kW/m^2 can facilitate oil desorption from the sorbent owing to the reduced oil viscosity. By contrast, light oil, such as diesel oil, demonstrates a minimal viscosity change between the initial and final points, indicating the minimal impact of heating on low-viscosity oil.

Oil sorption and desorption test

In the oil sorption test, both the PVDF and r-GONR oil sorbents exhibited comparable oil sorption capacities for motor oils 5 W-40 and 10 W-40, achieving approximately 19.5 ± 1.4 and 18.6 ± 0.5 g/g (Supplementary Fig. 4), respectively, which were attributed to their similar porosities (Table 1). However, when tested with diesel oil, the r-GONR oil sorbent demonstrated a slightly lower oil sorption capacity (11.5 ± 1.0 g/g) compared to the PVDF mat (14.5 ± 1.4 g/g). For practical applications, the oil sorption capacity was tested using synthesised oily wastewater that mimicked petrochemical industry effluents, including oil, water, total phosphorus (TP), and total nitrogen (TN). The oil sorption capacity using this simulated oily wastewater (18.0 ± 0.8 g/g) was comparable to that observed with an oil/water mixture containing only oil and water (18.3 ± 1.1 g/g). This similarity indicates that the presence of additional pollutants, such as TP and TN, did not significantly affect the sorption performance, as shown in Supplementary Fig. 4.

Subsequently, the oil-sorbed sorbents underwent desorption *via* Joule-heating and photothermal effects. The PVDF mats, with and without heating, exhibited low oil desorption capacities (normalised Q_d) for highly viscous oils, including motor oils 5 W-40 and 10 W-40, ranging from 1 to 0.86 ± 0.10 over 5 min (Fig. 3a, b) because of the tight adherence of oil to the sorbent. The introduction of heat *via* the Joule-heating and photothermal effects did not significantly improve oil desorption, resulting in efficiencies lower than 15% (Fig. 3d, e). Similarly, the r-GONR oil sorbent without heat showed oil desorption capacities (normalised Q_d values) due to the absence of heat effects, with efficiencies ranging from11.55 ± 0.68 to 15.33 ± 8.04%. In contrast to oil desorption without heat, both the r-GONR oil sorbent with Joule-heating effect (JH-r-GONR) and with photothermal effect (PT-r-GONR) exhibited rapid oil desorption rates for motor oils 5 W-40 and 10

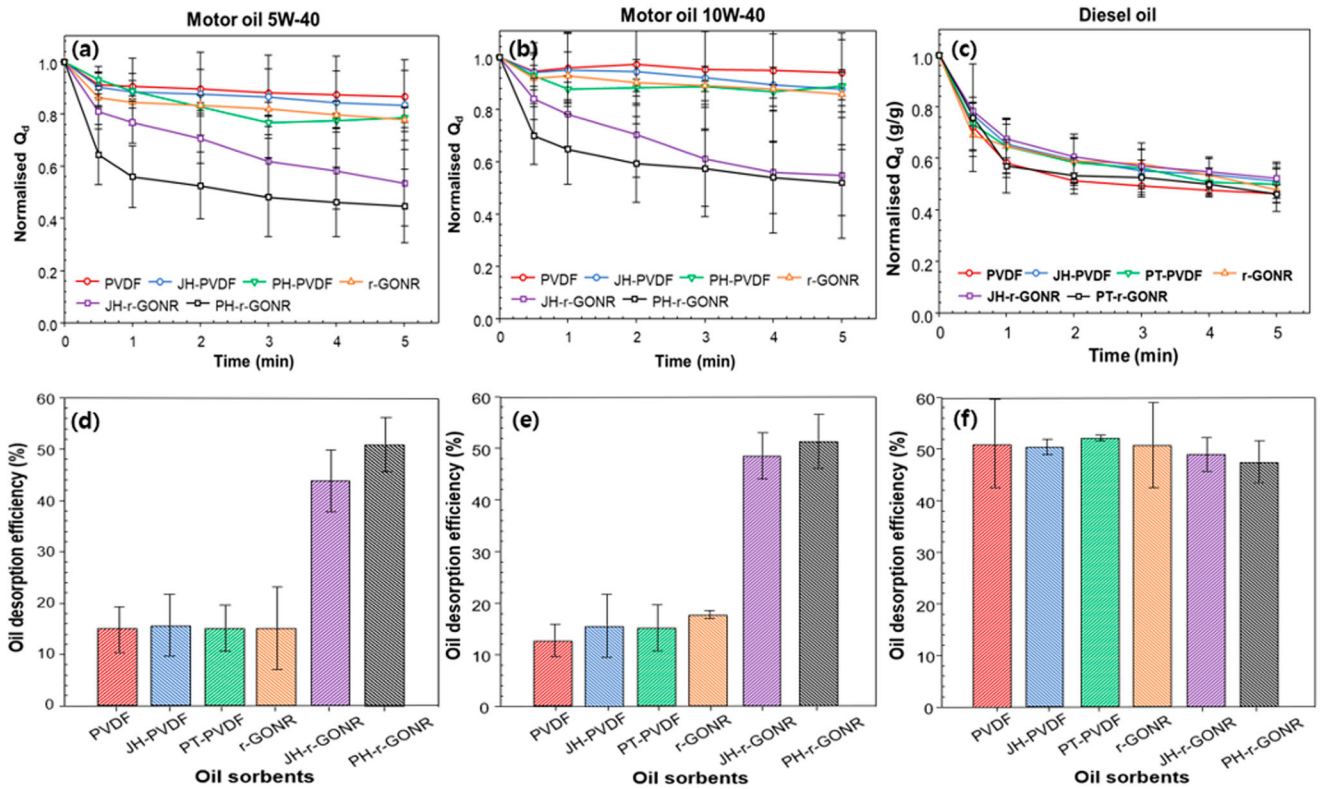

Fig. 3 | Oil desorption capacities and efficiency without heat and with heat including Joule-heating and photothermal effect. Oil desorption capacities of (**a**) motor oil 5W-40, (**b**) motor oil 10W-40, and (**c**) diesel oil, and oil desorption efficiencies of (**d**) motor oil 5W-40, (**e**) motor oil 10W-40, and (**f**) diesel oil (*Each error bar is defined as the standard deviation of the mean.).

W-40, reaching normalised Q_d values of 0.77 ± 0.08 and 0.78 ± 0.12, respectively, within 1 min. Subsequently, the oil desorption rates gradually decreased, resulting in high normalised Q_d values for both types of motor oils (Fig. 3a, b). The r-GONR oil sorbent with Joule-heating and solar-assisted heating demonstrated oil desorption efficiencies of $43.89 \pm 5.99\%$ and $51.15 \pm 5.26\%$, respectively, surpassing those of the PVDF mat and r-GONR oil sorbent without heat by more than threefold. This significant improvement in the oil desorption efficiency underscores the effectiveness of heat-assisted methods, highlighting the enhanced mobility of oil facilitated by heat in the r-GONR oil sorbent.

The PVDF and r-GONR oil sorbents demonstrated high normalised Q_d values for light oils, such as diesel oil, even without the application of heat (Fig. 3c). This high desorption efficiency can be attributed to the relatively low viscosity of the diesel oil compared with that of the highly viscous motor oils treated with heat (Fig. 3a, b). Upon the introduction of heat *via* Joule-heating and photothermal effects, the normalised Q_d values of both the PVDF and r-GONR oil sorbents remained comparable to those without heat. This consistency can be explained by the minimal impact of temperature on light oils such as diesel. Therefore, all oil sorbents exhibited an oil desorption efficiency of approximately 50%, as shown in Fig. 3f. In addition, the differences in desorption values between light oil and highly viscous oils under heat were not significant, owing to the viscosity reduction of the highly viscous oil.

Oil desorption mechanism with Joule-heating- and solar-assisted heating

Figure 4a illustrates the oil desorption mechanism using Joule-heating. When current flows through a conductive oil sorbent, collisions occur between phonons and accelerated electrons, resulting in simultaneous energy transfer to photons[50]. Therefore, Joule heat is generated, enhancing the electro-thermal performance of the oil sorbent fabricated in this study. Joule-heating occurred on the conductive surface, with continuous junction points[51]. However, the PVDF mat exhibited fewer junction points, reducing the number of electronic transport channels (Fig. 4b). By contrast, the r-GONR oil sorbent features more junction points, facilitating a continuous conductive interface and improving the electronic transport channels (Fig. 4c). Therefore, this phenomenon is expected to enhance the oil desorption capability.

The photothermal conversion mechanism is elucidated by the π-conjugated structure of r-GONR (Fig. 4d). When the r-GONR oil sorbent absorbs sunlight, electrons are transferred from the ground stage to an excited state because of the strong adsorption in the NIR spectrum of the r-GONR layer[52]. Subsequently, the absorbed NIR energy was released as heat, enabling the r-GONR oil sorbent to produce solar-assisted heating. This increased temperature enhances the oil desorption efficiency by weakening the adhesion force (van der Waals force) between the oil and sorbent[17]. Consequently, as the temperature of the oil and sorbent increased, the interaction between the oil and sorbent weakened, facilitating the easy desorption of oil from the sorbent.

Joule-heating- and solar-assisted reusability test

The recovery efficiencies of the highly viscous oils were evaluated through multiple oil sorption and desorption cycles. The PVDF mats underwent reusability testing up to the 4th cycle under the Joule-heating effect (JH-PVDF) and photothermal effect (PH-PVDF), as well as without heat (PVDF). However, they exhibited low recovery efficiencies for the motor oils 5 W-40 and 10 W-40 (<15%), rendering oil desorption impractical (Fig. 5a, b). In addition, their shapes and structures deteriorated after the 4th cycle compared to the initial state owing to their limited reusability and low mechanical strength (Supplementary Fig. 5 and Table 1). Similarly, the r-GONR oil sorbent without heat showed low recovery efficiencies below 15% owing to the absence of heat effects. However, unlike the PVDF mat, the r-GONR oil sorbent could be reused for up to 6th cycles owing to its improved mechanical strength (Fig. 5a, b)[53].

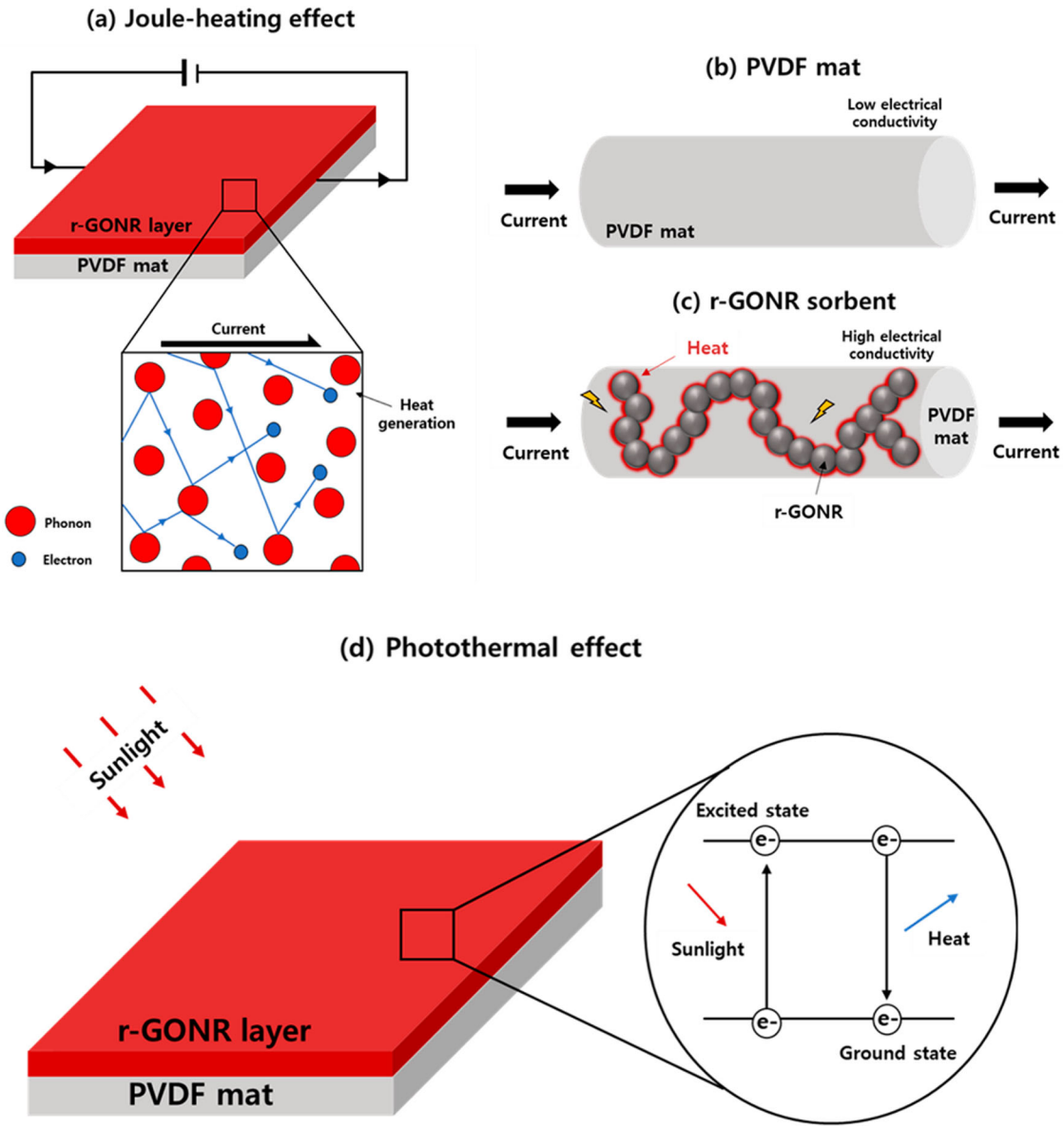

Fig. 4 | The mechanism of oil desorption and reuse, and generation of heat with Joule-heating effect. Schematic of (**a**) the mechanism of oil desorption from the sorbent using the Joule-heating effect, (**b**) the surface construction of the PVDF mat, (**c**) the surface construction of the r-GONR oil sorbent, and (**d**) the mechanism of oil desorption from the sorbent using the photothermal effect.

In comparison, the r-GONR oil sorbent with the Joule-heating effect (JH-r-GONR) exhibited superior reusability for highly viscous oils, extending up to the 5th sorption/desorption cycle, with an increased recovery efficiency of approximately 47%. However, beyond the 5th cycle, the recovery efficiency of JH-r-GONR rapidly decreases by up to 27% (approximately 1.7 times reduction) (Fig. 5a, b). As explained in section 3.2.2, this decrease can be attributed to the damage (burning) caused by severe collisions between phonons and electrons on the surface of the oil sorbent, as shown in Fig. 6a. Figure 6d shows the damage process of the r-GONR oil sorbent due to the Joule-heating effect. The current applied to the r-GONR oil sorbent also decreased in the 6th cycle (0.005 A) compared to the 1st cycle (0.014 A) at 25 V, owing to surface damage (Supplementary Fig. 6). Consequently, the recovery efficiency was dramatically reduced, making it challenging to reuse after the 6th cycle due to the reduced current and surface damage. By contrast, the r-GONR oil sorbent with photothermal effect (PH-r-GONR) could be used up to the 10th sorption/desorption cycle with stable recovery efficiencies for motor oils 5 W-40 and 10 W-40 (50.08 ± 4.51%–43.65 ± 5.02% and 51.58 ± 8.00-42.54 ± 2.27%, respectively) (Fig. 5a, b). The PH-r-GONR exhibited higher reusability than the JH-r-GONR owing to the indirect production of solar-assisted heating, which resulted in less surface damage. Figure 6b shows the surface of the sorbent after the 6th sorption/desorption cycle, indicating no damage and a clean surface with a high recovery efficiency of 51.2 ± 1.22% (no reduction compared to initial recovery efficiency). Although the recovery efficiency gradually decreased after the 6th cycle, reaching 43.65 ± 5.02% after the 10th cycle (roughly 1.16 times decrease) in Fig. 6c, the damage to the sorbent was less than that to JH-r-GONR. Therefore, the photothermal effect for oil desorption and sorbent reuse is expected to exhibit higher efficiency than other sorbent reuse methods, owing to its higher reuse time and high recovery efficiency.

Table 2 compares the reusability of the oil sorbent with the oil sorption capacity of the r-GONR-coated PVDF oil sorbent and other oil sorbents reported in the literature. The r-GONR-coated PVDF oil sorbent developed in this study demonstrated superior reusability, maintaining a high oil

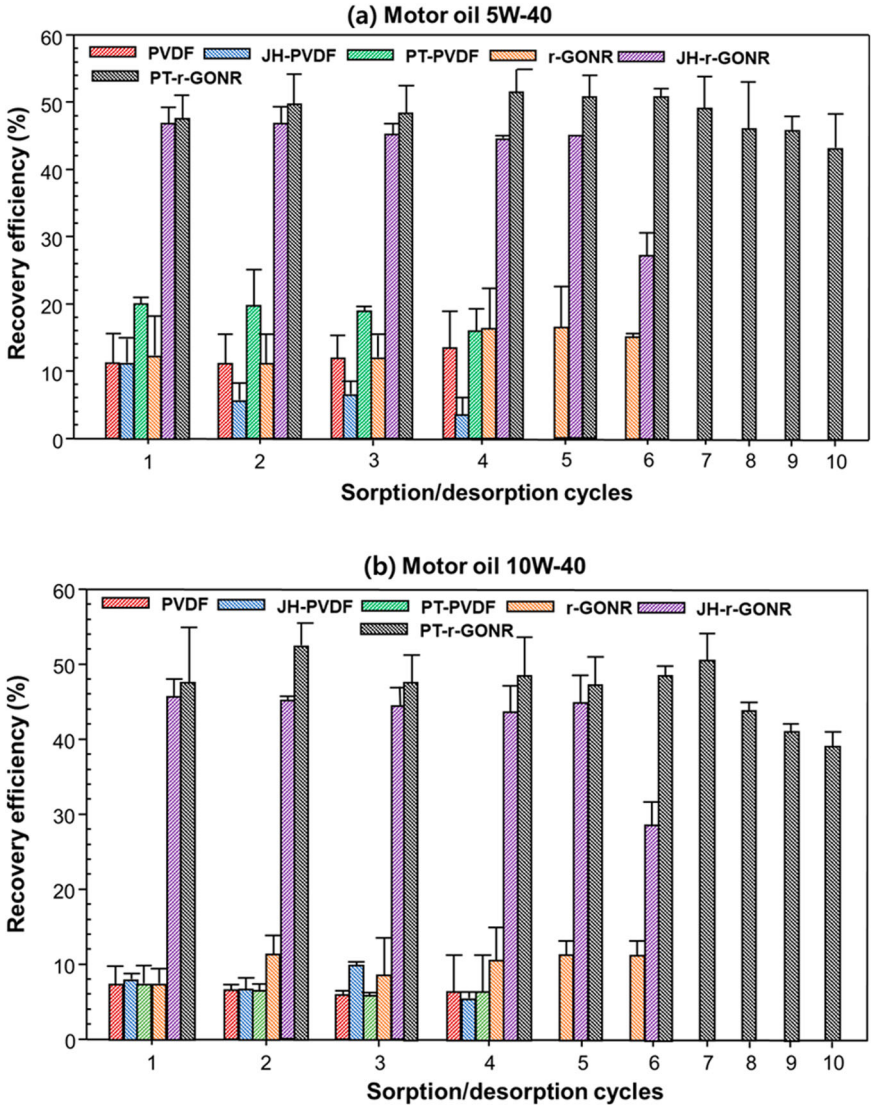

Fig. 5 | Recovery efficiency with highly viscous oils including Motor oil 5W-40 and 10W-40. Recovery efficiencies of (**a**) motor oil 5W-40 and (**b**) motor oil 10W-40 (*Each error bar is defined as the standard deviation of the mean.).

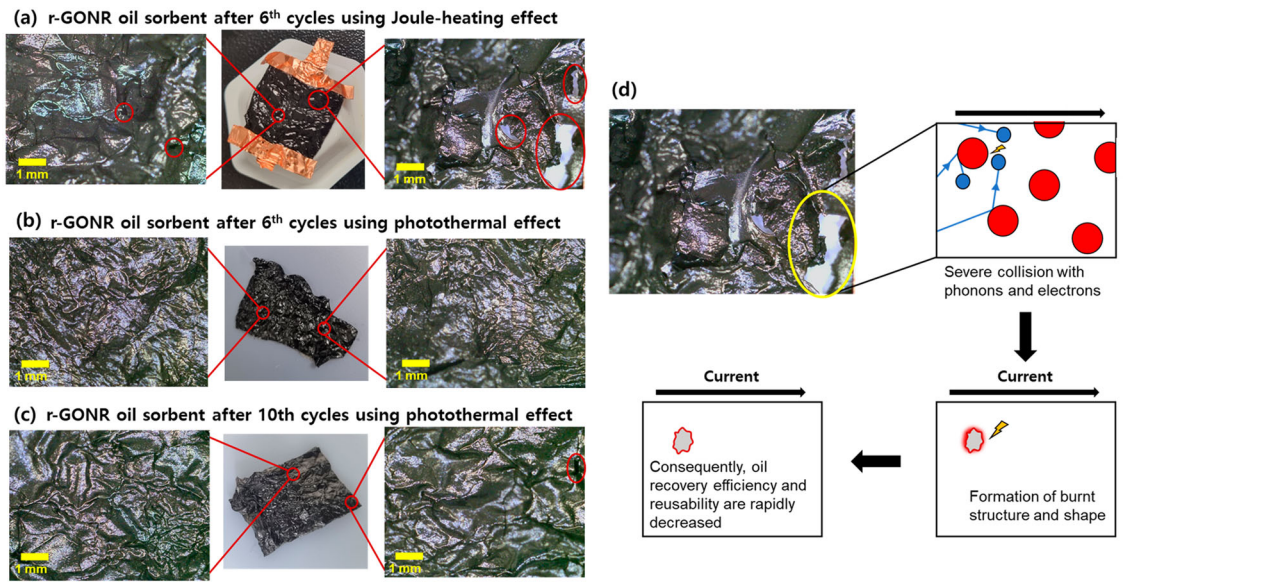

Fig. 6 | Surface images of the sorbent after reuse using Joule-heating and photothermal effect. Surface images of the sorbent after the reusability test: (**a**) after the 6th cycle using the Joule-heating effect, (**b**) after the 6th cycle using the photothermal effect, and (**c**) after the 10th cycle using the photothermal effect, along with a schematic showing the damage process of the sorbent using the Joule-heating effect.

Table 2 | Comparison of oil sorption capacity and reusability with various composite oil sorbents reported in the literature

Composite sorbent	Type of used oil	Oil sorption capacity	Reusability (cycle number)	Recovery method	Refs.
Liquefied lignin/PU foam	Highly viscous oil (light crude oil)	~7	-	-	61
Liquefied lignin/carbon nanotube/PU foam	Highly viscous oil (crude oil)	6.34	5	squeezing	15
Polyurethane sponge-reinforced silica aerogels based on tetraethoxysilane	Oil	10.6	5	Extraction using n-Hexane	62
r-GONR-coated PVDF oil sorbent	Highly viscous oil (10W-40 motor oil)	~19	5	Heat using Joule-heating effect	In this study
			10	Heat using photothermal effect	

sorption capacity (~19 g/g) throughout the 10th cycle, which was attributable to its effective photothermal effect.

Profitability evaluation

Figure 7 exhibits various economic aspects, including CapEx and OpEx, along with the costs of sorbent fabrication, revenue, and profit. The cost data inputs obtained from the experiments consisted primarily of machinery purchases and consumables used in the fabrication of the r-GONR oil sorbents. Based on the purchased equipment, a maximum of 17,520 units of the oil sorbents can be produced, as per the experimental results. These data served as the basis for estimating CapEx and OpEx (Fig. 7a), which were further utilised to model the economic parameters (Supplementary Table 1). Consequently, the costs of producing 1 m^2 of sorbents, including PVDF, JH-PVDF, PT-PVDF, r-GONR, JH-r-GONR, and PT-r-GONR, were estimated (Fig. 7b). It was observed that the CapEx of the oil sorbents with the Joule-heating effect was $278.83 higher than that of PVDF, r-GONR, and variants with photothermal effect (PT-PVDF and PT-r-GONR). Conversely, OpEx varied for all oil sorbents, primarily influenced by heating and the number of times the sorbent can be reused. Sorbent reuse implies that the cost is incurred once as OpEx, while the sorbent can be used multiple times, as demonstrated in the reusability tests (refer to section 3.3; where Joule-heating and photothermal-based sorbents can be used up to 5 and 10 times, respectively, with considerable oil recovery efficiencies for motor oil 5W-40 and 10W-40, and diesel oil). Consequently, the costs of fabricating oil sorbents of PVDF, JH-PVDF, PT-PVDF, r-GONR, JH-r-GONR, and PT-r-GONR were observed as $0.29, 0.29, 0.29, 0.34, 0.14, and 0.11 per m^2, respectively. The low cost of Joule-heating and photothermal-based oil sorbent fabrication was attributed to the lower OpEx based on the observed reuse.

Recovered oil represents a significant revenue source that is feasible even after offering oil spill cleanup services. Figure 7c shows the revenue from the oil sorbents based on the oil recovery rate results for the three types of oils (motor oil 5 W-40, motor oil 10-W, and diesel oil) tested (data related to revenue can be seen in Supplementary Table 2). The revenue from the oil sorbents was estimated based on the cost of recovered oil in the market ($4.833/L for motor oil 5W-40, $4.311/L for motor oil 10 W-40, and $1.062/L for diesel oil)[54–56]. Comparing the PVDF and r-GONR-based oil sorbents with and without heating, r-GONR oil sorbents with Joule-heating ($3.18–14.50/$m^2$) and photothermal ($6.37–29.00 /m^2) effects showed better revenues than PVDF and r-GONR oil sorbents without heat ($0.06–0.28/$m^2$ and $0.06–2.89/$m^2$, respectively). This was attributed to the superior oil sorption and desorption capacities and reusability of the fabricated r-GONR sorbents. Especially, PT-r-GONR showed the highest revenue owing to its high reusability up to the 10th cycle. Figure 7d shows the profits obtained using r-GONR oil sorbents with and without heat for oil recovery. The profits observed for the motor oil 5 W-40 recovery scenarios were 11.47%–21.70% higher than those for the 10 W-40 recovery scenarios. However, profits for the diesel oil recovery scenario were lower by 150.16% to 198.19% compared with motor oils 5 W-40 and 10 W-40, primarily for the abovementioned reasons. Notably, PT-r-GONR and JH-r-GONR demonstrated high profits compared to the others, mainly because of the low fabrication costs of PT-r-GONR and JH-r-GONR. By contrast, although the PVDF oil sorbents showed lower costs than the r-GONR oil sorbents, their similar reuse capabilities, and sorption and desorption capacities did not result in significant profits (the data related to revenues can be seen in Supplementary Table 2 of supplementary information).

Finally, the costs of the sorbents developed in this study were compared with those of the commercial PP sorbents. Based on the market prices, PP sorbent costs $7.7 to 8.16/$m^2$[257–59], significantly higher than all sorbent variants developed in this study. Additionally, considering OpEx based on the reuse time of the sorbents, the cost of commercial PP sorbents was $8/$m^2$ for single use, $40/$m^2$ for 5 reuse times, and $80/$m^2$ for 10 reuses. Overall, the cost of the sorbents developed in this study was lower than that of commercial sorbents, suggesting a high potential for commercialising r-GONR sorbents with Joule and photothermal heating effects.

Mitigated environmental impacts due to oil recovery

Using the methodology outlined in section 2.6, the mitigated environmental impacts were estimated for oil recovered using 1 m^2 of oil sorbents made of PVDF, JH-PVDF, PT-PVDF, r-GONR, JH-r-GONR, and PT-r-GONR. Initially, for a functional unit of 1 kg, the midpoint indicators estimated using the ReCiPe Midpoint (H) life cycle impact assessment method were colleFcted for both motor oil (assuming motor oil 5 W-40 and 10 W-40 are equivalent for simplicity in the environmental assessment) and diesel oil; a detailed list of 18 indicators and their corresponding values are shown in Supplementary Table 3 in the Supplementary Information. Given the applications of the sorbents in this study, specific indicators were selected (Fig. 8a), including climate change, fossil depletion, freshwater ecotoxicity, marine ecotoxicity, and water depletion. Figure 8b–f show the quantified mitigated environmental impacts of the oil recovered from the PVDF and r-GONR oil sorbents, with and without Joule-heating and photothermal effects. The mitigation indicators underscore the significant environmental threats posed by motor oil spills. Although the scores for diesel oil were lower than those for motor oil, both types of oils represented significant environmental hazards, emphasising the critical role of sorbents. Comparing the sorbent variations, the mitigation potential was particularly high for PT-r-GONR (more than 2 times), followed by JH-r-GONR and r-GONR. Therefore, PT-r-GONR can reduce severe damage to aquatic ecosystems and human health owing to their ability to mitigate freshwater and marine ecotoxicity as well as water depletion. Additionally, it can minimise societal losses because improved environmental impact mitigation leads to decreased treatment costs for oil clean-up.

Methods

Fabrication of heatable oil sorbents

To synthesise heatable oil sorbents, a PVDF solution (Molecular Weight = 45,500 g/mol, CAS no.:24937–79-9) with a concentration of 20

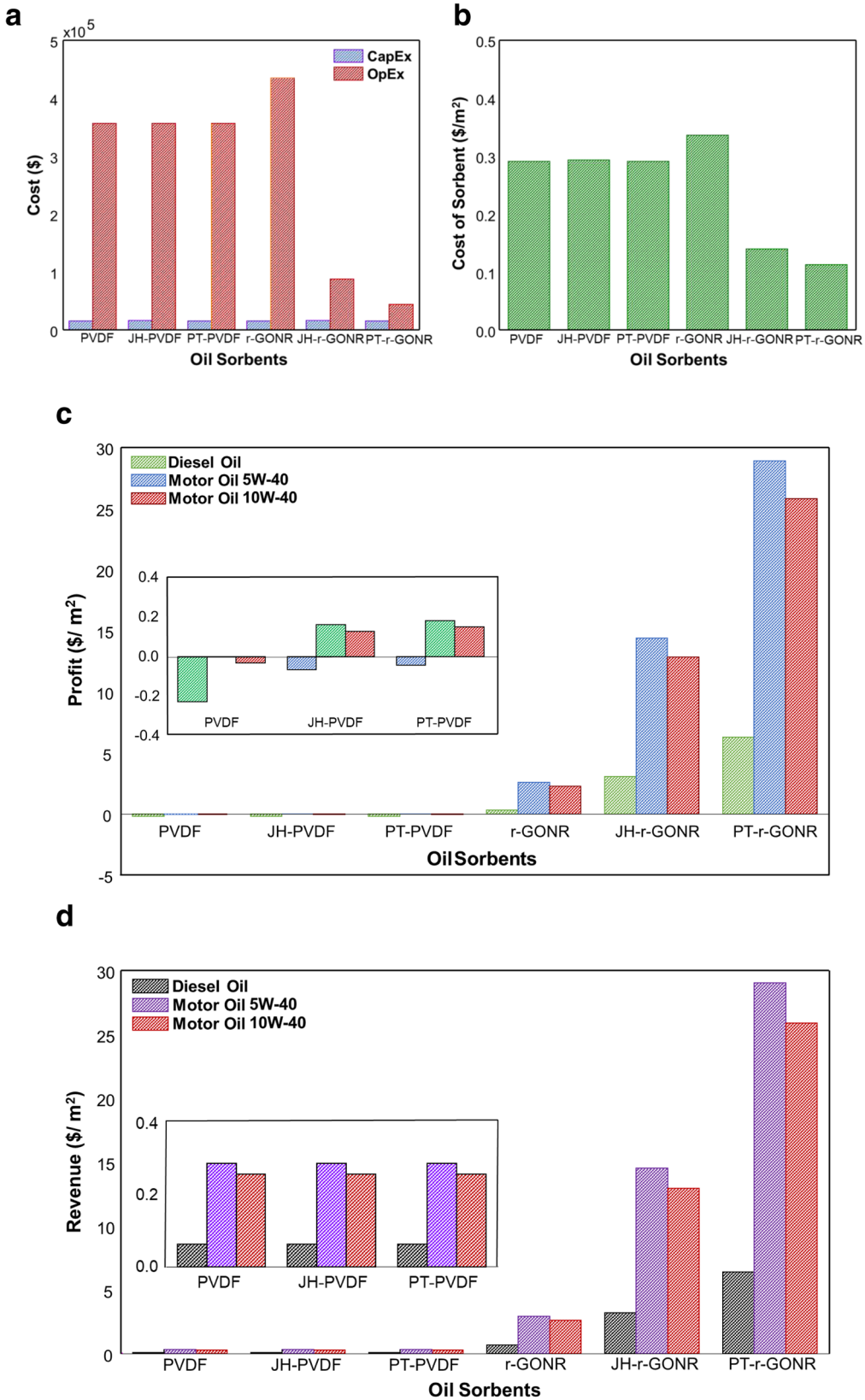

Fig. 7 | Economic factors with the PVDF and r-GONR oil sorbents with and without Joule-heating and photothermal effects. a CapEx and OpEx, (**b**) cost of the sorbents fabricated, (**c**) revenues using motor oil 5W-40, motor oil 10W-40, and diesel oil recovery, and (**d**) profits using motor oil 5W-40, motor oil 10W-40, and diesel oil recovery.

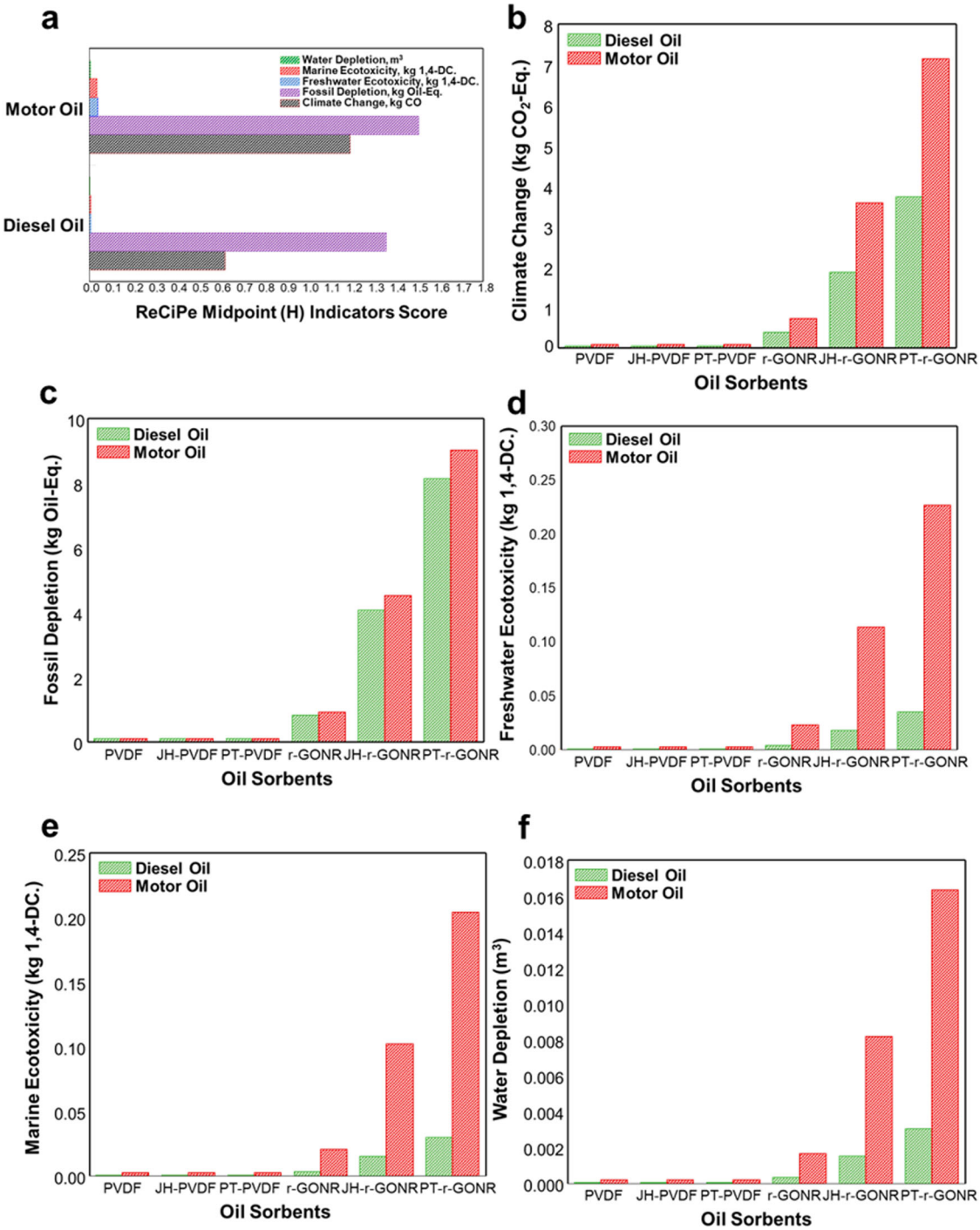

Fig. 8 | Mitigated environmental impacts due to motor oil and diesel recovery using the PVDF and r-GONR oil sorbents with and without Joule-heating and photothermal effect. a Selected midpoint indicators for motor oil and diesel oil estimated based on ReCiPe Midpoint (H) life cycle impact assessment method, *note: data for all the indicators is provided in the supplementary information*, (**b**) Mitigated climate change in kg CO_2-Eq., (**c**) Mitigated fossil depletion in kg Oil-Eq., (**d**) Mitigated freshwater ecotoxicity in kg 1,4-DC., (**e**) Mitigated marine ecotoxicity in kg 1,4-DC., and (**f**) Mitigated water depletion. Note: detailed results of 18 midpoint indicators are given in Tables S4 and S5 of supplementary information.

wt.% was prepared. This solution was dissolved in a solvent mixture of N, N-dimethylformamide (DMF, anhydrous, ≥99.8%, CAS no.:68-12-2) and acetone (ACS reagent, ≥99.5%, CAS no.:67-64-1) in a weight ratio of 8:2 and stirred with a magnetic stirrer overnight. The PVDF mat was then fabricated *via* electrospinning under the following optimised conditions: voltage of 13 kV, flow rate of 0.8 mL/h, working distance of 15 cm, and room temperature with a relative humidity of 40%.

To enhance the electrical conductivity and thermal resistance, the GONR was coated onto a PVDF mat using a two-step coating process. Initially, GONRs with 5 wt.% concentration were dispersed in methanol (Duksan, CAS no.: 67-56-1) for 30 min. The GONR dispersion was then applied to the PVDF mat using dip coating for 1 d, followed by spray coating for 1–2 min with a spray gun (U-star S-130, China), maintaining a working distance of 5 cm between the gun and the surface. This method ensured

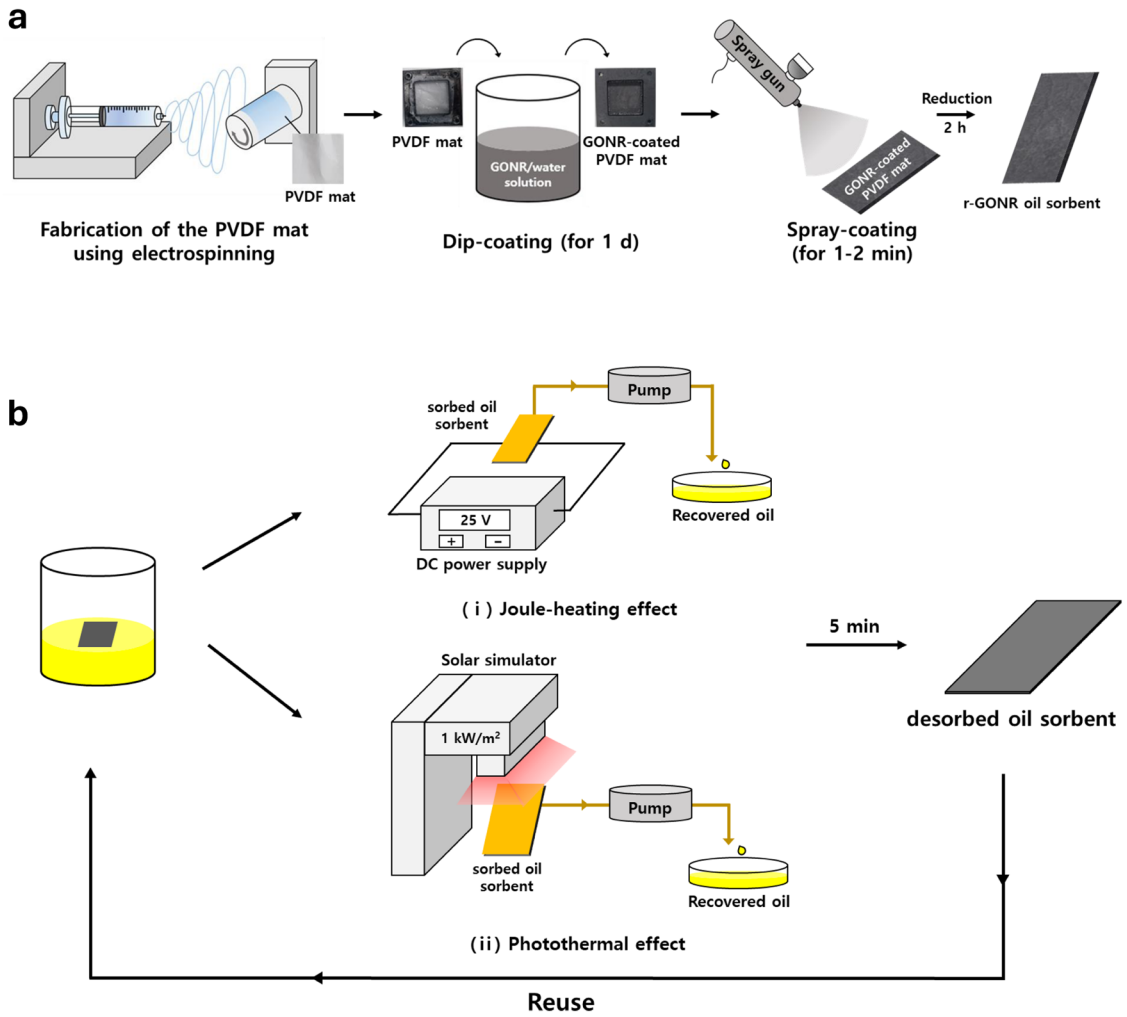

Fig. 9 | Process of fabrication of r-GONR oil sorbent, and oil desorption and reuse test. Schematic of (**a**) fabrication of r-GONR oil sorbent and (**b**) the oil desorption and reuse process of the r-GONR-coated oil sorbents: **b-(i)** Joule-heating effect and **b-(ii)** photothermal effect.

Table 3 | Viscosity and density values of different oils used in this study

Oil	Viscosity (mPa·s)	Density (g/m^3)
Motor oil (10W-40)	124	0.872
Motor oil (5W-40)	76	0.875
Diesel oil	1	0.732

uniform coverage of GONR on the sorbent. GONRs were synthesised by the longitudinal unzipping of MWCNT, as described in our previous study[17], at an optimised concentration of 5% to achieve excellent electrical conductivity and resistivity. Following coating, the oil sorbent was chemically reduced using 3% hydrazine (Sigma Aldrich, CAS no.:10217-52-4) for 4 h to enhance its hydrophobicity. Before use, all oil sorbents were dried in ambient air at approximately 25 °C overnight. Figure 9a shows a schematic of the r-GONR oil sorbent fabrication process.

Oil sorption test

The oil sorption capacity was assessed using a synthesised oil/water mixture consisting of 10 mL oil and 50 mL deionised (DI) water. To evaluate the oil sorption capacity of the simulated real oily wastewater, we synthesised an oil–water mixture that mimicked petrochemical industry effluents. This comprised 10 mL of oil, 50 mL of water, 1.23 mg of TP, and 101.2 mg of TN, with a pH range of 6.5 to 9.1 and a temperature range of 18.3 to 22.4 °C[60].

The PVDF and r-GONR oil sorbents were immersed in an oil–water mixture for 1 h to ensure sufficient oil sorption. Subsequently, the oil was drained for 20 s to determine the precise amount of oil sorbed. The oils tested included highly viscous oils such as motor oils (5 W-40 and 10 W-40) and diesel oil as a lighter oil for comparison. Motor oils were chosen as substitutes for crude oil, which is difficult to obtain due to regulatory constraints. The viscosities and densities of the oils are presented in Table 3. The oil sorption capacity was calculated by measuring the mass difference between the dry and wet sorbents, using Eq. (1):

$$Q_s = \frac{m - m_0}{m_0}, \tag{1}$$

where Q_s is the maximum oil-sorption capacity (g/g), m is the mass of the oil sorbent after sorption (g), and m_0 is the initial mass of the oil sorbent (g). Each test was conducted three times to ensure the reproducibility of the results.

Desorption and reusability test using Joule-heating and photothermal effects

To evaluate the reusability of the oil sorbent, oil desorption tests were conducted using the Joule-heating effect with a direct current power supply (IT6720, Itech, Taiwan) and a peristaltic pump, as illustrated in Fig. 9b-(i). These tests were performed at 25 V for 5 min to allow the oil-desorption capacity to reach equilibrium. Subsequently, the oil-sorption test was

Table 4 | Oil sorbents with oil desorption technologies

Name	Used sorbents	Desorption technologies	Desorption time
PVDF	PVDF	-	5 min
JH-PVDF		Joule-heating (at 25 V)	
PT-PVDF		Photothermal (under 1 kW/m^2)	
r-GONR	r-GONR	-	
JH-r-GONR		Joule-heating (at 25 V)	
PT-r-GONR		Photothermal (under 1 kW/m^2)	

repeated using the oil-sorbed sorbent, and the reusability of the sorbent was determined by iteratively conducting sorption and desorption tests. Each test was conducted three times to ensure the reproducibility of the results. The PVDF mat and r-GONR oil sorbents, without heat and with the Joule-heating effect, were designated PVDF, JH-PVDF, r-GONR, and JH-r-GONR, respectively. The oil sorbents were evaluated using specific desorption technologies and times, as shown in Table 4.

The reusability was assessed based on the mass of the sorbents between sorption and desorption using Eq. (2):

$$R = \frac{m - m_d}{m - m_0} \times 100\,(\%), \tag{2}$$

where R represents the reusability of the sorbent (%); m and m_d denote the mass of the oil sorbent after sorption and desorption (g), respectively; and m_0 is the initial mass of the oil sorbent (g).

An oil-desorption test had conducted using the photothermal effect with a solar simulator (LS150; ABET Technologies, USA). After oil sorption, the sorbents were exposed to solar irradiation (1 kW/m^2) for 5 min. Subsequently, the oil sorbents were immersed in an oil–water mixture to determine their oil sorption capacity after desorption. Reusability was also calculated using the equation provided above (Eq. 2). All experiments were conducted at least three times to ensure reproducibility of the results. Figure 9b-(ii) presents a schematic illustrating the oil desorption and reuse process of the heatable oil sorbent, highlighting the role of the photothermal effect. The PVDF mat and r-GONR oil sorbents, both without heat and with a photothermal effect, were denoted as PVDF, PT-PVDF, r-GONR, and PT-r-GONR, respectively, as shown in Table 4.

Characterisation

The morphologies and structures of the oil sorbents were examined using field-emission SEM (FE-SEM, Gemini500, Zeiss, Germany). After reusability with Joule-heating and photothermal effects, the surface images of the oil sorbents were observed using a digital microscope (DIMIS-M, Siwon, Republic of Korea). To validate the coating of r-GONRs on the sorbent, changes in the chemical composition were investigated using SEM-EDS and Fourier transform infrared spectroscopy (FTIR, Nicolet iN10MX, Thermo Fisher Scientific, US) in the range of 4000 to 600 cm^{-1}. The wettability of the sorbents with oil and water was assessed using a contact angle analyser (DSA25E, Kruss, Germany). For porosity measurements, the sorbents were immersed in 1-butanol (ACS reagent, ≥99.4%, CAS no.:71-36-3) for 1 h, and the pore volume was calculated using the obtained wet and dry weights of the oil sorbents. The changes in surface temperature due to heat were recorded using a thermal imager (Tis75 + , Fluke, USA) for 5 min. Viscosities of the oil were analysed using a rheometer (Dhr2, Ta Instruments, USA) with different oil temperatures ranging from 20 to 100 °C. To investigate the mechanical stability, the tensile strength was measured using a universal testing machine (UTM; RB 301 Unitech-M, R&B, Republic of Korea).

Economic feasibility assessment

A techno-economic feasibility analysis was conducted by calculating the revenue earned through oil recovery and estimating the cost of fabricating the PVDF and r-GONR oil sorbents with and without Joule-heating and photothermal effects. The revenues from the recovered motor oils (5 W-40 and 10 W-40) and diesel oil were also estimated using Eq. (3).

$$Revenue = ROQ_i \times MPO_i, \tag{3}$$

where ROQ is the recovered oil quantity in litres (L), MPO is the market price of the recovered oil in $/L, and i represents the type of oil recovered.

Equation (4) was used to estimate the fabrication costs of the PVDF and r-GONR oil sorbents with and without Joule-heating and photothermal effects.

$$\begin{aligned} &Cost\ of\ Sorbent\ Fabrication \\ &= \frac{\left[CapEx + (\mathrm{OpEx} \times F_{CR,i,n}) + (\mathrm{Rep} \times F_{SF,i,n}) - (\mathrm{Sal} * F_{SF,i,n})\right] \times \mathrm{F_{CR,I,n}}}{Total\ no.of\ sorbents\ units\ produced}, \end{aligned} \tag{4}$$

where $CapEx$ is the capital cost in $; $OpEx$ is the operational cost in $, Rep is the replacement cost in $; Sal is the salvage cost paid back after the end-of-life in $; $F_{\mathrm{CR,I,n}}$ is the capital recovery factor estimated using $F_{CR,i,n} = \frac{i(i+1)^n}{(1+i)^n - 1}$; $F_{\mathrm{SF},i,n}$ is the sinking fund factor estimated using $F_{SR,i,n} = \frac{i}{(1+i)^n - 1}$; i is the interest rate (%), and n is the lifetime. The detailed calculations are presented in Supplementary Table 1.

Mitigated Environmental Impacts

The mitigated environmental impacts were estimated using Eq. (5).

$$MEI = ROQ_i \times EI_i, \tag{5}$$

where ROQ is the recovered oil quantity in litres (L) and EI represents the environmental impact indicators estimated based on the ReCiPe Midpoint (H) life cycle impact assessment method utilising the eco-invent database. The data are shown in Supplementary Table 3, where i denotes the type of oil recovered.

Data availability

All data will be made available on request.

Received: 24 June 2024; Accepted: 6 September 2024;
Published online: 17 September 2024

References

1. statista. Oil consumption worldwide from 1970 to 2022, https://www.statista.com/statistics/265261/global-oil-consumption-in-million-metric-tons/ (2023).
2. Jha, M. N., Levy, J. & Gao, Y. Advances in remote sensing for oil spill disaster management: state-of-the-art sensors technology for oil spill surveillance. *Sensors* **8**, 236–255 (2008).
3. Baig, N., Abdulazeez, I. & Aljundi, I. H. Low-pressure-driven special wettable graphene oxide-based membrane for efficient separation of water-in-oil emulsions. *Npj Clean Water* **6**, https://doi.org/10.1038/s41545-023-00252-y (2023).
4. Cao, R. C., Chen, H. B., Rong, Z. R. & Lv, X. Q. Impact of ocean waves on transport of underwater spilled oil in the Bohai Sea. *Mar. Pollut. Bull.* **171**, 112702 (2021).
5. Asif, Z., Chen, Z., An, C. J. & Dong, J. X. Environmental impacts and challenges associated with oil spills on shorelines. *J. Mar. Sci. Eng.* **10**, https://doi.org/10.3390/jmse10060762 (2022).
6. Chang, S. E., Stone, J., Demes, K. & Piscitelli, M. Consequences of oil spills: a review and framework for informing planning. *Ecol. Soc.* **19**, https://doi.org/10.5751/ES-06406-190226 (2014).
7. Gupta, S. & Tai, N. H. Carbon materials as oil sorbents: a review on the synthesis and performance. *J. Mater. Chem. A* **4**, 1550–1565 (2016).

8. Bayat, A., Aghamiri, S. F., Moheb, A. & Vakili-Nezhaad, G. R. Oil spill cleanup from sea water by sorbent materials. *Chem. Eng. Technol.* **28**, 1525–1528 (2005).
9. Byun, S., Lee, J., Lee, J. & Jeong, S. Reusable carbon nanotube-embedded polystyrene/polyacrylonitrile nanofibrous sorbent for managing oil spills. *Desalination* **537**, https://doi.org/10.1016/j.desal.2022.115865 (2022).
10. Bayik, G. D. & Altin, A. Conversion of an industrial waste to an oil sorbent by coupling with functional silanes. *J. Clean. Prod.* **196**, 1052–1064 (2018).
11. Ye, Q. et al. Metal-organic framework modified hydrophilic polyvinylidene fluoride porous membrane for efficient degerming selective oil/water emulsion separation. *Npj Clean Water* **5**, https://doi.org/10.1038/s41545-022-00168-z (2022).
12. Sun, X. F., Sun, R. C. & Sun, J. X. Acetylation of rice straw with or without catalysts and its characterization as a natural sorbent in oil spill cleanup. *J. Agr. Food Chem.* **50**, 6428–6433 (2002).
13. Wei, Q. F., Mather, R. R. & Fotheringham, A. F. Oil removal from used sorbents using a biosurfactant. *Bioresour. Technol.* **96**, 331–334 (2005).
14. El-Din, G. A., Amer, A. A., Malsh, G. & Hussein, M. Study on the use of banana peels for oil spill removal. *Alex. Eng. J.* **57**, 2061–2068 (2018).
15. Hwang, U. et al. Hydrophobic lignin/polyurethane composite foam: An eco-friendly and easily reusable oil sorbent. *Eur. Polym. J.* **165**, https://doi.org/10.1016/j.eurpolymj.2021.110971 (2022).
16. Allen, C. The Economic and Environmental Benefits of Efficient Waste Management. *Adv. in Recycl. & Waste Manag*. **8**, 1–2 (2023).
17. Byun, S., Park, S., Lee, E. J., An, A. K. & Jeong, S. Joule-heating electrospun reduced-graphene oxide nanoribbon-coated reusable polymeric sorbent with an excellent sorption/desorption of high-viscosity oils. *Carbon* **219**, 118826 (2024).
18. Li, Z. D. et al. Easily fabricated low-energy consumption joule-heated superhydrophobic foam for fast cleanup of viscous crude oil spills. *Acs Appl Mater. Inter* **13**, 51652–51660 (2021).
19. Wang, Y. et al. Solar-heated graphene sponge for high-efficiency clean-up of viscous crude oil spill. *J. Clean. Prod.* **230**, 995–1002 (2019).
20. Yaghi, B. M. & Al-Bemani, A. Heavy crude oil viscosity reduction for pipeline transportation. *Energ. Sour.* **24**, 93–102 (2002).
21. Wu, X. W. et al. Photothermal and Joule heating-assisted thermal management sponge for efficient cleanup of highly viscous crude oil. *J. Hazard Mater.* **403**, 124090 (2021).
22. Li, Z. D. et al. Facile fabrication of solar-heating and Joule-heating hyperelastic MXene-modified sponge for fast all-weather clean-up of viscous crude oil spill. *J. Hazard Mater.* **448**, 130930 (2023).
23. Li, Z. D., Lin, Z. P., Qiu, F. X., Uyama, H. & Zhang, T. Energy-optimized oil spill cleanup: joule-/solar-heating copper foam for efficient all-weather recovery of viscous crude oil. *Ind. Eng. Chem. Res*. https://doi.org/10.1021/acs.iecr.3c01690 (2023).
24. Qi, B. H. et al. Melt-blown fiber felt for efficient all-weather recovery of viscous oil spills by Joule heating and photothermal effect. *J. Hazard Mater.* **460**, 132523 (2023).
25. Li, Z. D., Lin, Z. P., Tian, Q., Qiu, F. X. & Zhang, T. Solar-heating superhydrophobic modified melamine sponge for efficient recovery of viscous crude oil. *J. Hazard Mater.* **440**, 129799 (2022).
26. Ahmed, F. E., Ibrahim, Y. & Hilal, N. A spacer-based approach for localized Joule heating in membrane distillation. *Npj Clean Water* **7**, https://doi.org/10.1038/s41545-024-00337-2 (2024).
27. Zeng, G. J. et al. Solar-assisted efficient cleanup of high-viscosity oil spills using magnetic porous biochar. *J. Alloy Compd.* **924**, https://doi.org/10.1016/j.jallcom.2022.166474 (2022).
28. Bansal, P., Vineyard, E. & Abdelaziz, O. Status of not-in-kind refrigeration technologies for household space conditioning, water heating and food refrigeration. *Int. J. Sustain. Built Environ.* **1**, 85–101 (2012).
29. Kitanovski, A. & Egolf, P. W. Innovative ideas for future research on magnetocaloric technologies. *Int. J. Refrig* **33**, 449–464 (2010).
30. Niu, H. F., Li, J. B., Qiang, Z. & Ren, J. Versatile and cost-efficient cleanup of viscous crude oil by an elastic carbon sorbent from direct pyrolysis of a melamine foam. *J. Mater. Chem. A* **9**, 11268–11277 (2021).
31. Ku, B. J. et al. Photothermal fabrics for efficient oil-spill remediation via solardriven evaporation combined with adsorption. *Acs Appl. Mater. Inter* **13**, 13106–13113 (2021).
32. Zhang, C., Liang, H. Q., Xu, Z. K. & Wang, Z. K. Harnessing solar-driven photothermal effect toward the water-energy nexus. *Adv. Sci.* **6**, 1900883 (2019).
33. Majumder, S., Meher, A., Moharana, S. & Kim, K. H. Graphene nanoribbon synthesis and properties in polymer composites: a review. *Carbon.* **216**, 118558 (2024).
34. Wang, P. L., Ma, C., Yuan, Q., Mai, T. & Ma, M. G. Novel TiCT MXene wrapped wood sponges for fast cleanup of crude oil spills by outstanding Joule heating and photothermal effect. *J. Colloid Inter. Sci.* **606**, 971–982 (2022).
35. Xia, D., Li, H. & Huang, P. Understanding the Joule-heating behaviours of electrically-heatable carbon-nanotube aerogels. *Nanoscale Adv.* **3**, 647–652 (2021).
36. Fan, T. T. et al. Robust Graphene@PPS fibrous membrane for harsh environmental oil/water separation and all-weather cleanup of crude oil spill by joule heat and photothermal effect. *Acs Appl. Mater. Inter* **13**, 19377–19386 (2021).
37. Wang, B. et al. High-efficiency and all-weather crude oil spill remediation by an eco-friendly self-heating MXene-coated poly(butylene adipate-co-terephthalate) porous monolith. *J. Clean Prod.* **417**, https://doi.org/10.1016/j.jclepro.2023.137983 (2023).
38. Huang, W., Zhang, L., Lai, X. J., Li, H. Q. & Zeng, X. R. Highly hydrophobic F-rGO@wood sponge for efficient clean-up of viscous crude oil. *Chem. Eng. J.* **386**, https://doi.org/10.1016/j.cej.2019.123994 (2020).
39. Huang, J., Tang, T. Q. & He, Y. R. Coupling photothermal and Joule-heating conversion for self-heating membrane distillation enhancement. *Appl. Therm. Eng.* **199**, https://doi.org/10.1016/j.applthermaleng.2021.117557 (2021).
40. Guo, X. X., Gao, H., Wang, S. Y., Yin, L. F. & Dai, Y. R. Scalable, flexible and reusable graphene oxide-functionalized electrospun nanofibrous membrane for solar photothermal desalination. *Desalination* **488**, https://doi.org/10.1016/j.desal.2020.114535 (2020).
41. Ding, Y. J. et al. Multifunctional three-dimensional graphene nanoribbons composite sponge. *Carbon* **104**, 133–140 (2016).
42. Raji, A. R. O. et al. Composites of graphene nanoribbon stacks and epoxy for joule heating and deicing of surfaces. *Acs Appl. Mater. Inter.* **8**, 3551–3556 (2016).
43. Xie, H. Q., Chen, L. F., Yu, W. & Wang, B. Q. Temperature dependent thermal conductivity of a free-standing graphene nanoribbon. *Appl. Phys. Lett.* **102**, https://doi.org/10.1063/1.4796177 (2013).
44. Jun, Y. S. et al. Enhanced electrical and mechanical properties of graphene nanoribbon/thermoplastic polyurethane composites. *Carbon* **174**, 305–316 (2021).
45. Akhavan, O., Ghaderi, E. & Emamy, H. Nontoxic concentrations of PEGylated graphene nanoribbons for selective cancer cell imaging and photothermal therapy. *J. Mater. Chem.* **22**, 20626–20633 (2012).
46. Cho, K. M. et al. Ultrafast-selective nanofiltration of an hybrid membrane comprising laminated reduced graphene oxide/graphene oxide nanoribbons. *Acs Appl. Mater. Inter* **11**, 27004–27010 (2019).
47. Choi, Y. et al. Graphene oxide nanoribbon hydrogel: viscoelastic behavior and use as a molecular separation membrane. *Acs Nano* **14**, 12195–12202 (2020).

48. Cai, T., Wang, R., Neoh, K. G. & Kang, E. T. Functional poly(vinylidene fluoride) copolymer membranes surface-initiated thiol-ene click reactions. *Polym. Chem.* **2**, 1849–1858 (2011).
49. Yu, H. et al. Enhanced power output of an electrospun PVDF/MWCNTs-based nanogenerator by tuning its conductivity. *Nanotechnology* **24**, 405401 (2013).
50. Yang, X. et al. Multifunctional magnetic sponge with outstanding solar/electro-thermal performance for high-efficiency and all-day continuous cleanup of crude oil spills. *Sci. Total Environ.* **892**, 164601 (2023).
51. Yang, Y., Guo, Z & Liu, W. Multifunctional Polypyrrole/Mxene-Wrapped Sponge with Synergistic Solar and Joule-Heating Effect for Efficient Adsorption and All-Weather Recovery of Crude Oil. *Chem. Eng. J.* **485**, 149927 (2023).
52. Cai, C. L., Wang, T., Zhang, Y. X. & He, N. Y. Facile fabrication of ultra-large graphene film with high photothermal effect and thermal conductivity. *Appl. Surf. Sci.* **563**, https://doi.org/10.1016/j.apsusc.2021.150354 (2021).
53. Tabarraei, A., Shadalou, S. & Song, J. H. Mechanical properties of graphene nanoribbons with disordered edges. *Comp. Mater. Sci.* **96**, 10–19 (2015).
54. Walmart. *Mobil 1 FS European Car Formula Full Synthetic Motor Oil 5W-40, 5 Quart*, https://www.walmart.com/ip/Mobil-1-FS-European-Car-Formula-Full-Synthetic-Motor-Oil-5W-40-5-Quart/437059473 (2024).
55. direct, H. *20ltr Ultra Euro 10w-40 - 40-20 - TFUD20L - M403D117*, https://hgvdirect.co.uk/10w-40-euro-5-synthetic-low-saps-diesel-engine-oil-20-l.html (2024).
56. EIA. *U.S. Regular Gasoline Prices*(dollars per gallon)*, https://www.eia.gov/petroleum/gasdiesel/ (2024).
57. ONE, A. *AS ONE Laminated Liquid Absorption Mat (For Water, Oil and Solvents)and others*, https://cacheby.com/@cacheby/products/cce50296-6881-11ec-90d6-0242ac120003?srsltid=AfmBOoreWjCJPOqIrANAcaB1_d0RTEVNr2E9Ze_PlbqyIRruGkDXmxElq54 (2024).
58. 3M. *Petroleum Sorbent Pads, Oil Only, 19" x 17", 38 gal. Absorbancy*, https://www.tenaquip.com/product/3m-petroleum-sorbent-pads-oil-only-19-x-17-387-gal-absorbancy-hp-156-sgv450?3MCC=true (2024).
59. Brady. *Brady Spill Response Plus Universal Plus Absorbent Pad*, https://cacheby.com/@cacheby/products/Brady-Spill-Response-Plus-Universal-Plus-Absorbent-Pad-hhkqud0fg0?srsltid=AfmBOooF8qh8kRkFlczQBODtvXw5eEMT2BUmy5K1CulipNlw8YdEhBdCmD0 (2024).
60. Wei, Y., Jin, Y. & Zhang, W. J. Treatment of high-concentration wastewater from an oil and gas field via a paired sequencing batch and ceramic membrane reactor. *Int. J. Environ. Res. Public Heath* **17**, 1953 (2020).
61. Mohammadpour, R. & Sadeghi, G. M. M. Effect of liquefied lignin content on synthesis of bio-based polyurethane foam for oil adsorption application. *J. Polym. Environ.* **28**, 892–905 (2020).
62. Li, M., Jiang, H. Y. & Xu, D. Preparation of sponge-reinforced silica aerogels from tetraethoxysilane and methyltrimethoxysilane for oil/water separation. *Mater. Res. Express* **5**, https://doi.org/10.1088/2053-1591/aab7c3 (2018).

Acknowledgements

This work was supported by the Korea Agency for Infrastructure Technology Advancement (KAIA) grant funded by the Ministry of Land, Infrastructure, and Transport (RS-2022-00144137), the Basic Science Research Program through the National Research Foundation of Korea (NRF) funded by the Ministry of Education (2022R1C1C1006877), and the Korea Institute for Advancement of Technology (KIAT) grant funded by the Korean Government (MOTIE) (P0017310, Human Resource Development Program for Industrial Innovation (global)). This work was partially supported by the Research Grant Council (RGC) of Hong Kong (GRF 11218122 and 11209421).

Author contributions

Siyoung Byun: Investigation, Methodology, and Writing– Original Draft; Muhammad Usman Farid: Methodology, Writing– Review and Editing; Nallapaneni Manoj Kumar: Investigation, Methodology, Writing– Original Draft, Data Analysis, and Writing– Review and Editing; Shauhrat S. Chopra: Writing– Review and Editing; Sangyong Nam: Resources, Methodology; Alicia Kyoungjin An: Supervision, Writing– Review and Editing; Sanghyun Jeong: Funding Acquisition, Supervision, Writing– Review and Editing.

Competing interests

The authors declare no competing interests.

Additional information

Supplementary information The online version contains supplementary material available at https://doi.org/10.1038/s41545-024-00387-6.

Correspondence and requests for materials should be addressed to Alicia Kyoungjin An or Sanghyun Jeong.